Shear behaviour of one-way high strength plain and FRC slabs reinforced with basalt FRP bars

Abathar Al-Hamrani, Wael Alnahhal[*]

Department of Civil and Architectural Engineering, Qatar University, Doha, Qatar

ARTICLE INFO

ABSTRACT

The purpose of this study is to investigate the shear behavior of high-strength one-way plain and basalt fiber reinforced concrete (BFRC) slabs reinforced with basalt fiber reinforced polymers (BFRP) bars. A total of 8 slabs having 2550 mm length, 600 mm width and 150 mm height were tested under four-point loading until failure. The main test variable was the BFRP longitudinal reinforcement ratio with two ratios of 0.792 % and 1.27 %. Also, two slabs were cast with basalt macro fibers (BMF) at a volume fraction (V_f) of 0.75 % to explore the effect of the added fibers on the shear capacity of the tested one-way slabs. Following the experimental testing, the shear capacities of the BFRC-BFRP one-way slabs were evaluated analytically using two approaches. The first approach considers the individual contribution of concrete and BMF to shear strength, while the second takes into account a direct alteration to the concrete contribution owing to the addition of BMF. The experimental results showed that the shear capacity was enhanced by 25 % to 29 % when the reinforcement ratio was increased from 0.792 % to 1.27 %. In addition, the shear capacity of the slab containing 0.75 % of BMF was notably enhanced over the plain concrete slab, however, this enhancement was less notable when a higher reinforcement ratio was used. Based on the analytical investigation, a new model that accounts for the individual contribution of concrete and the BMF is proposed. The model has accurately and conservatively predicted the experimental data with a mean experimental to predicted shear capacity of 1.10 and a coefficient of variation of 7.95 %.

1. ntroduction

Bridge decks and parking garages have recognized as examples of structures where the application of deicing salts causes corrosion in the steel reinforcement [1]. Such a problem can be addressed by using the non-corrosive fiber-reinforced polymer (FRP) bars. Due to the lower elastic modulus of FRP bars than that of steel bars, larger mid-span deflections accompanied with wider and deeper cracks were reported in concrete members reinforced with FRP bars[2–6]. This will reduce the contribution to shear strength from several shear resisting mechanisms; such as aggregate interlock, the residual tension in the cracked concrete, and the uncracked concrete in the compression zone. Meanwhile, the current codes and design guidelines [7–10] recommended the reinforced concrete (RC) members with FRP bars to be over-reinforced, and hence, determining the shear capacity is crucial as the members will be vulnerable to shear failure[11].

To address the brittle character of shear, as well as having brittle FRP bars with linear-elastic stress–strain behavior, fiber-reinforced concrete

(FRC) might be considered an effective approach for improving the ductility and shear capacity of FRP-RC elements. Several studies have investigated the effect of adding steel fibers on the shear behavior of conventional RC beams [12–18]. Their test results revealed an enhanced shear capacity with better post-cracking behavior that was associated with less brittle failure. More recent studies have studied the effect of adding basalt macro fibers (BMF) on shear behavior of FRP-RC beams [19–21]. For instance, Mohaghegh et al. [19] found that FRP-FRC beams made with 0.5 % and 1 % volume fractions (V_f) of BMF experienced 25 % and 45 % increase in their ultimate shear capacities over the plain concrete beams, respectively. A notable enhancement in the shear capacity was also noticed by El Refai et al. [21] due to the addition of 0.75 % and 1.5 % V_f of BMF. Furthermore, the integration of basalt fibers in concrete has demonstrated an improved mechanical properties [22] and a decrease in crack widths owing to the proactive action of fibers upon concrete cracking [19–21,23,24] and as a result, the shear resistance produced from the aggregate interlock may be sustained for a longer length of time.

Table 1
Concrete mixture proportions.

	Volume Fractions of BMF(% V_f)	
	0.0 %	0.75 %
Cement (kg/m³)	500	500
Water (kg/m³)	165	165
Sand 0/4.75 mm, (kg/m³)	700	700
Gabbro coarse aggregate, 10 mm (kg/m³)	105	105
Gabbro coarse aggregate, 20 mm (kg/m³)	945	945
Basalt macro fibers (kg/m³)	0	14.25
Superplasticizer (kg/ m³)	0.35	0.37

Traditionally, research on one-way FRP-RC slabs has focused on the flexural behaviour [25–30], with just limited attempts to investigate their shear behavior [1,11,31]. For example, El-Sayed et al. [1] have investigated the shear strength of one-way concrete slabs reinforced with either GFRP or CFRP bars. The authors reported that the shear capacity was increased by 36 % and 44 % as the reinforcement ratio ρ was increased from 0.39 % to 1.18 % and 0.86 % to 1.71 %, respectively. In addition, CFRP-RC one-way slabs showed a 24 % higher shear strength than their counterparts reinforced with GFRP bars. Similar findings were reported by Abdulsalam et al. [11] who observed that the elastic modulus of the utilized FRP bars had a substantial impact on the shear behavior of FRP-RC one-way slabs. A recent work by Chang and Seo [26] reported that steel RC one-way slabs experienced higher stiffness and lower deflection and strains than their counterparts reinforced with GFRP bars.

Considering the aforementioned reported literature on the lower elastic modulus of FRP bars compared to steel, their linear elastic behavior up to failure, their low dowel capacity, and the brittleness of concrete and its weak resistance to tensile stresses, investigating the shear behavior of one-way FRP-RC slabs must be given critical attention. A review of the literature revealed that there is no single study that investigates the shear behavior of one-way slabs reinforced with BFRP bars, whilst few studies that investigate their flexural behavior [29,30]. Furthermore, previous studies mainly evaluated the shear behavior in terms of plain concrete, with no research examining the effect of macro-fibers on the shear strength of one-way FRP RC slabs. This study aims to fill this research gap by experimentally and analytically investigating the shear behavior of plain and BFRC one-way slabs reinforced with BFRP bars. Finally, an analytical model was suggested to predict the shear capacity of plain and BFRC one-way slabs reinforced with BFRP bars.

2. Experimental program

2.1. Materials

Two batches of concrete were made. One of the two mixes was made with basalt macro fibers (BMF) added at a volume fraction (V_f) of 0.75 %, and the other mix was made without fibers as a control. The mix proportions for both mixes are listed in Table 1. The BMF is shown in Fig. 1a with a total length (l_f), diameter (d_f), and density of 43 mm, 0.66 mm, and 1900 kg/m³, respectively. According to the manufacturer's datasheet [32]; the tensile strength (σ_f) and the modulus of elasticity (E_{fiber}) were 1000 MPa and 45 GPa, respectively. A total of eight slabs each was made with identical dimensions of 2550 mm length, 150 mm

Table 2
Material Properties for the used bars.

Material Properties	Sand-coated BFRP bars	Ribbed BFRP bars	Sand-coated GFRP bars	Steel bars
Diameter of the bar (mm)	11.35	11.9	12	12
Yield strength (MPa)	–	–	–	578
Ultimate Tensile Strength (MPa)	1177	1100	1030	726
Ultimate strain %	2.55	2.2	2.36	14
Elastic Modulus (GPa)	49.48	50	47	200

Table 3
Testing matrix.

Specimen ID	Bar type	Reinforcement ratio ρ%	ρ/ρ_b	The volume fraction of BMF%
SCB-ρ1-0 %	BFRP	0.792	2.27	0
RB-ρ1-0 %	BFRP		ρ_b	0
SCG-ρ1-0 %	GFRP			0
SCB-ρ1-0.75 %	BFRP			0.75
S-ρ1-0 %	Steel		0.24	0
			ρ_{bs}	
SCB-ρ2-0 %	BFRP	1.27	3.62	0
RB-ρ2-0 %	BFRP		ρ_b	0
SCB-ρ2-0.75 %	BFRP			0.75

ρ_{bs} = balanced reinforcement ratio for steel.

(a) (b)

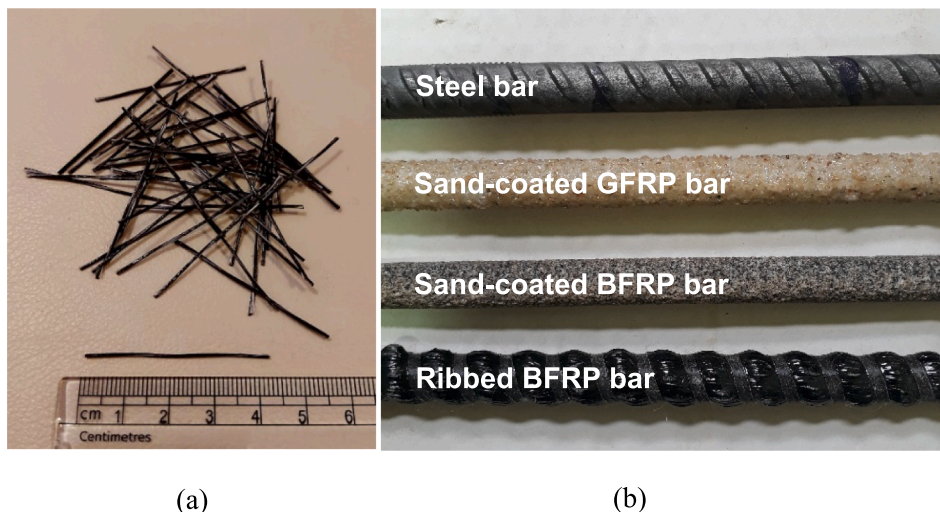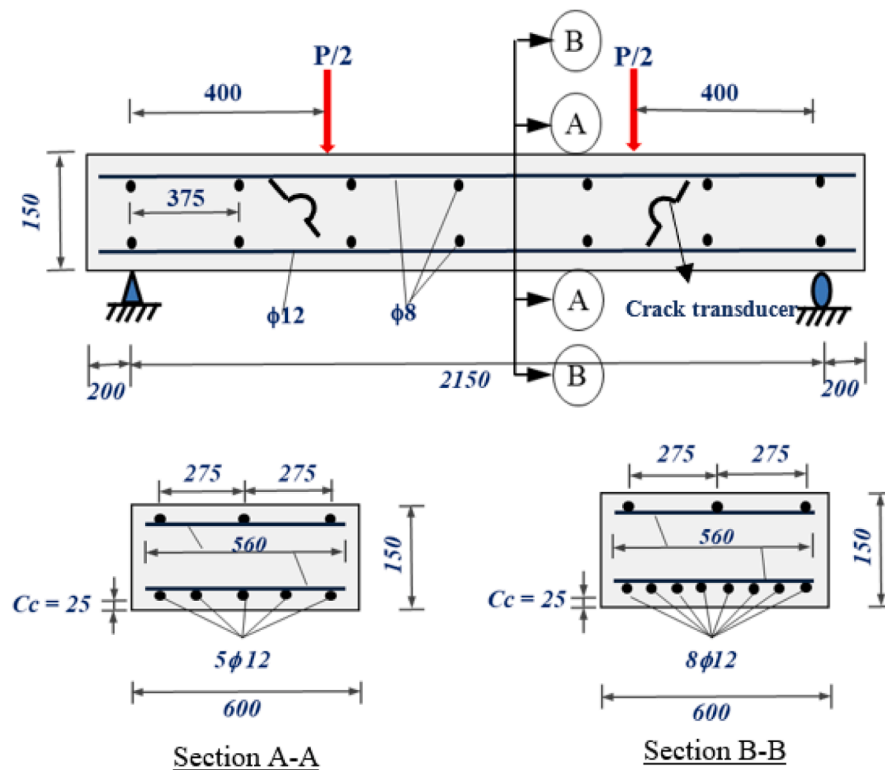**Fig. 1.** (a) BMF; (b) longitudinal bars.

Fig. 2. One-way slab testing set-up: (a) schematic drawing with dimensions in mm; (b) photo for test set-up.

height, and 600 mm width were cast using either basalt fiber reinforced concrete (BFRC) or plain concrete mix. Four slabs were reinforced with sand-coated BFRP bars and two slabs were reinforced with ribbed BFRP bars to compare the surface treatment effect, whereas the remaining two slabs, one was reinforced with sand-coated GFRP bars and one with steel bars to serve as control slabs. Fig. 1b presents the different types of longitudinal bars used in this study. The tensile properties of the tested bars were evaluated according to ASTM D7205[33], and are listed in Table 2.

The labeling of each slab shown in Table 3 composed of three different terms that refer to the studied parameters. The terms ('SCB', 'RB', 'SCG' or 'S') refer respectively to the type of longitudinal reinforcement as sand-coated basalt, ribbed basalt, sand-coated glass, or steel. The second term refers to the main longitudinal reinforcement

ratios (ρ_1 and ρ_2), which were designed to be greater than the balanced reinforcement ratio (ρ_b) with the values of 2.27 ρ_b, and 3.62 ρ_b, respectively. The third term represents the volume fraction of BMF used in the concrete mix (0 %, 0.75 %), which corresponds to the plain concrete mix with no fibers and the BFRC mix with 14.25 kg/m^3 of BMF, respectively. The slabs designation and the detailed test variables are summarized in the testing matrix shown in Table 3.

2.2. Test setup and procedure

The testing setup and the slabs configuration are presented in Fig. 2. All slabs were loaded monotonically up to failure under a four-point loading system at a stroke-controlled rate of 1 mm/min. To capture the strain in concrete and bottom reinforcement, each slab was

Table 4
Compressive and flexural strength results for concrete mixtures.

	Avg compressive Strength (MPa)	Avg Flexural Strength (MPa)	f_{600}^D	f_{150}^D
Plain concrete	55.12	4.29	–	–
0.75 % BFRC	55.33	5.17	4.4	0.5

f_{600}^D: stress value corresponding to a net deflection $= \dfrac{\text{span length}}{600}$.

f_{150}^D: stress value corresponding to a net deflection $= \dfrac{\text{span length}}{150}$.
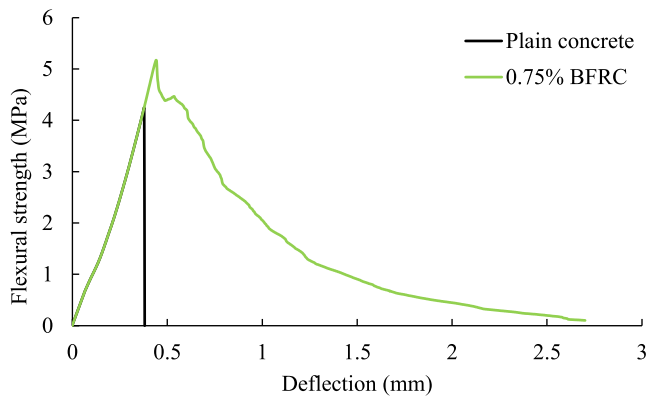

Fig. 3. Residual flexural tensile strength of concrete with 0.75% of BMF vs plain concrete.

instrumented with four electrical strain gauges, two were placed at the middle compression zone of concrete and two at the middle of the bottom reinforcements. Besides, two linear variable differential transformers (LVDTs) were installed in the middle of the slab to capture the maximum deflection. The shear cracks width was measured via two crack transducers each was installed diagonally at the mid-height of two shear spans as can be seen in Fig. 2a. Different numbers of flexural reinforcing bars were used on the bottom side of the tested slabs, namely *5ϕ12* mm bars and *8ϕ12* mm bars corresponding to ρ_1 and ρ_2 as shown in Fig. 2a in sections A-A and B-B, respectively.

3. Results and discussion

3.1. Compressive and flexural strengths

The compressive and flexural strengths were determined by preparing four cylinders and prisms from each mix of sizes 200×100 mm and $500 \times 100 \times 100$ mm and testing them according to ASTM C39 [34] and ASTM C1609 [35] guidelines, respectively. The compression and flexural test results are listed in Table 4. It can be seen that the fiber

content had no apparent effect on the compressive strength. Similarly, other publications [36,37] concluded that the influence of steel fibers on the compressive strength of high strength concrete was insignificant. On the other hand, the added BMF recorded an increase of 17 % in the flexural tensile strength over the plain concrete prism. Furthermore, the plain concrete prisms experienced a sudden failure after reaching the maximum flexural strength, while in the post-cracking stage, the prisms with BMF experienced residual tensile strength represented by f_{600}^D and f_{150}^D values that corresponds to 4.4 MPa and 0.5 MPa at midspan deflections of 0.5 mm and 2 mm, respectively as shown in Fig. 3. Thus, the toughness (T_{150}^D) and the equivalent flexural strength ratio $(R_{T,150}^D)$ of the BFRC prisms were determined to equal 13 Joule and 38 % compared to 2.43 Joule and 9 % for the pain concrete prisms, respectively.

3.2. The shear test results

The experimental results of the tested slabs are summarized in Table 5. In the following sections, a detailed discussion will be carried out on the effect of the studied parameters on the load–deflection behavior, the load–strain behavior, the shear capacity, and the failure modes and cracks pattern.

3.2.1. Load-deflection behavior

As can be seen from Fig. 4, which summarizes the load–deflection diagrams of the tested slabs, all curves constituted bilinear behavior namely the pre-cracking and post-cracking stages. Approximately no clear difference in stiffness was observed in the pre-cracking stage. This is because the load is mainly resisted by concrete in this stage and the slabs were functioning with their full inertia. In Fig. 4a, the slabs reinforced with SCB, SCG, or RB bars have shown almost similar behavior, whereas as expected the slab reinforced with steel bars showed an evident higher stiffness due to the higher elastic modulus of steel than the FRP bars. The cracking load in all slabs was recorded at a range of 21.5 kN to 32.5 kN. Slabs with a higher reinforcement ratio of 1.27 % have shown a higher cracking load than slabs with a lower reinforcement ratio of 0.792 %. The same observation was noticed for slabs with 0.75 % BMF compared to plain concrete slabs. For example, slab RB-ρ2-0 %, with higher reinforcement ratio, cracked at 27.5 kN compared to its counterpart slab RB-ρ1-0 % that cracked at 21.5 kN. Furhermore, slab SCB-ρ2-0.75 %, with V_f = 0.75 % cracked at 32.5 kN while its counterpart slab SCB-ρ2-0 % with no fibers cracked at 22.5 kN. In the post-cracking stage, Fig. 4a shows that there is a slightly lower stiffness of slab SCB-ρ1-0 % compared to slabs RB-ρ1-0 % and SCG-ρ1-0 %. This could be attributed to the small difference in the bar diameters between the SCB, the RB, and the SCG bars, as indicated in Table 2. Another possible reason for the slight difference in stiffness could be the different surface textures of the used bars, which imply different bond behavior with the surrounding concrete. Fahmy et al. [38] stated that the helically ribbed BFRP bars had attained much higher ultimate bond strength than that of the sand-coated BFRP bars[38]. Having this in mind, in addition

Table 5
Experimental results of the tested slabs.

Beam designation	Ultimate load (P/2) (kN)	Δ_{Max} (mm)	Maximum Strain		Load at initial bending crack (kN)	V_{cr} (kN)	Failure type	Angle of failure
			Longitudinal bars	Concrete				
SCB-ρ1-0 %	69.82	37.08	0.0071	0.0016	22.5	32.5	DT	45
RB-ρ1-0 %	76.18	37.46	0.0076	0.0016	21.5	31.5	DT	48
SCG-ρ1-0 %	82.96	39.81	0.0087	0.0018	23.5	34.5	DT	43
S-ρ1-0 %	109.62	92.04	0.015	0.0033	32	40	SY + CC	–
SCB-ρ1-0.75 %	81.48	43.52	0.009	0.0015	25.5	40	DT	41
SCB-ρ2-0 %	90.08	35.52	0.0081	0.0014	22.5	37.5	DT	47
RB-ρ2-0 %	95.65	27.86	0.0062	0.0015	27.5	38	DT	38
SCB-ρ2-0.75 %	93.55	31.62	0.0076	0.0016	32.5	43.5	DT	36

DT = diagonal tension failure; SY = steel yielding; CC = concrete crushing; V_{cr} = load at first shear crack; Δ_{Max}=Maximum midspan deflection.

(a) Effect of reinforcement type

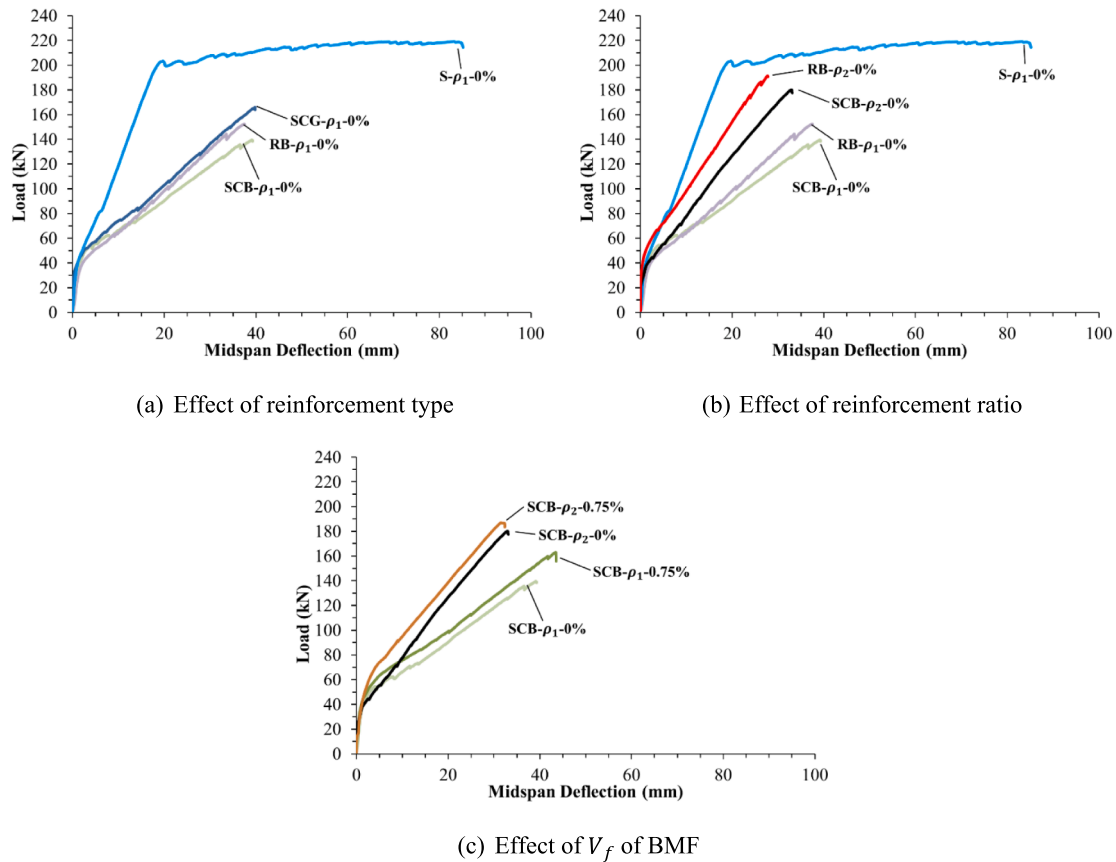(b) Effect of reinforcement ratio

(c) Effect of V_f of BMF

Fig. 4. Load vs deflection behavior of the tested slabs.

to the slightly bigger diameter, which provides a higher surface area for friction with the surrounding concrete, may justify the higher stiffness obtained in Fig. 4a. Furthermore, since the cracked slabs have utilized the reduced inertia of concrete section, slabs with higher reinforcement ratios or with $V_f = 0.75$ % have shown higher stiffness than slabs with lower reinforcement ratios or with no fibers at the same loading level as shown in Fig. 4b and 4c, respectively. This is because the inclusion of a higher reinforcement ratio has significantly improved the flexural stiffness as the developed cracks were resisted by a more number and a higher area of reinforcing bars. This is also could be attributed to the effectiveness of BMF, which restricts cracks propagation and widening, resulting in reduced deflection in the post-cracking stage.

3.2.2. Load-strain behavior

The load versus midspan strain behavior in both concrete and the reinforcing bars for all slabs can be depicted in Fig. 5. Prior to the first flexural crack in the concrete, the strain values were negligible. Upon cracking, a clear increase in strain values was noted. This increase was more notable in FRP-RC slabs than in steel-RC slab due to the low modulus of elasticity of FRP bars as indicated in Fig. 5a. However, as shown in Fig. 5b and 5c, this increase was mitigated in slabs with higher reinforcement ratios or with added BMF, respectively. The strain values of FRP-RC slabs then continued to increase linearly up to failure load. On the other hand, once the linear stage reached the end in the steel-RC slab, the steel started yielding resulting in higher strain values at the same loading level. While the ultimate strain values of longitudinal bars and concrete in FRP-RC slabs were recorded in the range of 6200 to 9000 microstrain (με) and 1400 to 1800 με, respectively, the strain values in the steel-RC slab were recorded as 15,000 με and 3300 με. The higher strain values are related to the higher ultimate loading capacity and deflection attained by the steel-RC slab. Also, as shown in Fig. 5b, the strain values for concrete and FRP bars at the same loading level were

less in slabs with a higher reinforcement ratio. Compared to slabs RB-ρ2-0 % and SCB-ρ2-0 % which have BFRP bar strains of 2300 με and 3850 με at a loading level of 100 kN, the measured strains in the counterpart slabs RB-ρ1-0 % and SCB-ρ1-0 % were 4840 με and 5440 με, respectively. It is also observed that slabs with $V_f = 0.75$ % experienced lower strains than their counterpart slabs with no fibers. As an example, slab SCB-ρ2-0.75 % has FRP strain of 3300 με at a loading level of 100 kN, while the strain in slab SCB-ρ2-0 % was 3900 με. This could be attributed to the presence of BMF across the flexural cracks, which in turn acts as a second reinforcement that slows the cracks widening and reduces slabs deflection and strain values.

3.2.3. Failure modes and cracks pattern

All FRP-RC slabs have experienced diagonal tension shear failure, whereas the steel-RC slab has experienced a steel yielding followed by concrete crushing at the loading point. The failure modes along with the crack patterns are shown in Fig. 6. The vertical crack formation was initiated at the extreme tension fiber in the mid-span of the slabs. With the increase in the applied load, the vertical cracks propagated toward the extreme compression fiber, and adjacent cracks started to develop between the two-point loads. After that, vertical cracks began to develop at the shear spans near the point loads, and as the applied load increased, more vertical cracks developed along the shear span. The vertical cracks then started to incline as they get closer to the neutral axis owing to the high shearing stress effect on the neutral axis of the slabs. Due to the dominance of shear stresses, the inclined cracks kept propagating toward the loading point leading to shear failure. Prior to failure, the bottom tip of the critical shear crack was observed to extend horizontally parallel to the longitudinal reinforcement level as can be observed in several slabs shown in Fig. 6. This phenomenon could be attributed to the relatively smooth fractured surface of high-strength concrete [2,39–41], which leads to a less contribution of the aggregate
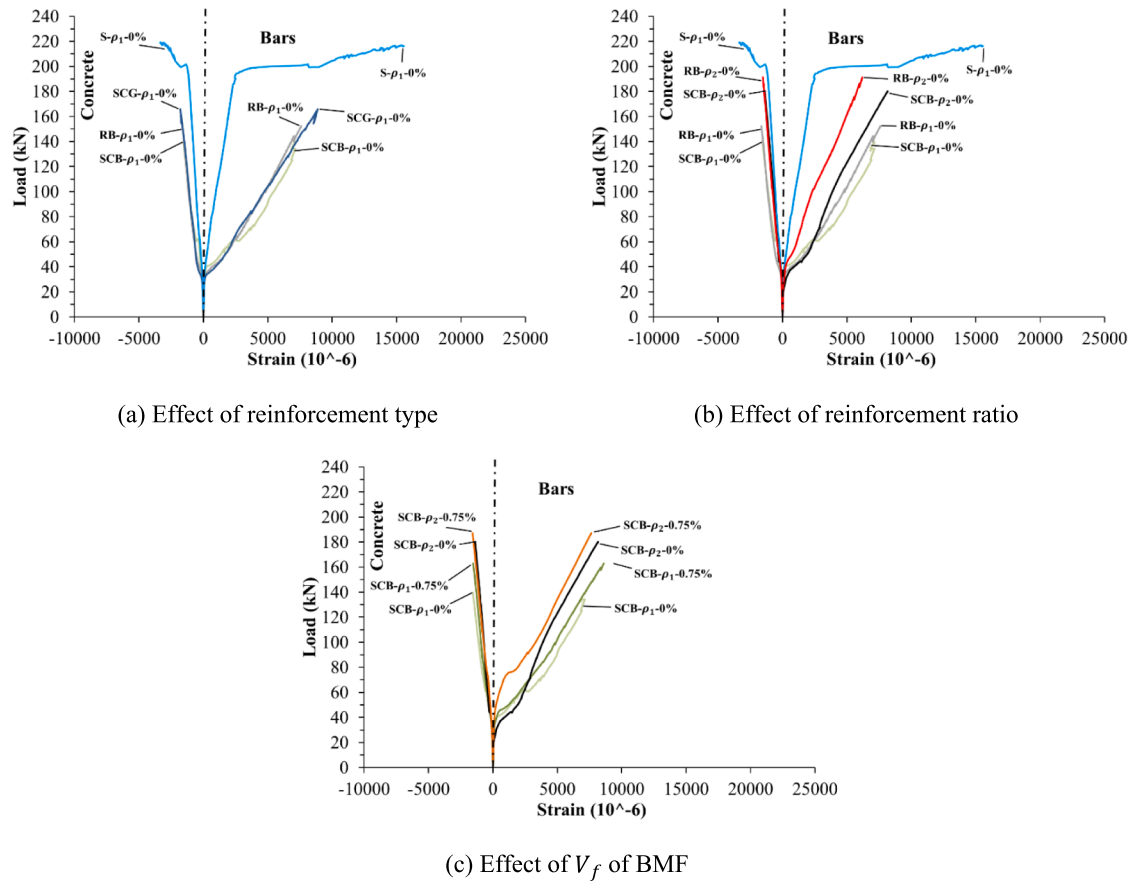
(a) Effect of reinforcement type

(b) Effect of reinforcement ratio

(c) Effect of V_f of BMF

Fig. 5. Load vs bar and concrete strains behavior.

interlock in transferring shear stresses. According to El-Sayed et al. [2], this lower contribution caused higher dowel forces in the longitudinal reinforcing bars across the crack. The dowel forces in addition to the existed bond stresses surrounding the longitudinal bars have exceeded the tensile strength of concrete causing horizontal cracks to be formed at the longitudinal reinforcement level [2]. This observation was also reported by Abdul-Salam et al. [11].

Shear cracks were developed at a range from 31.5 kN to 34.5 kN in slabs having a reinforcement ratio of 0.792 %, whereas they were developed at a range from 37.5 kN to 43.5 kN in slabs having a reinforcement ratio of 1.27 %. Additionally, shear cracks were also observed to be delayed in BFRC slabs. As an example, the shear cracks in slabs SCB-ρ1-0 % and SCB-ρ2-0 % occurred at 32.5 kN and 37.5 kN, whereas they were delayed to 40 kN and 43.5 kN in slabs SCB-ρ1-0.75 % and SCB-ρ2-0.75 %, respectively, as shown in Figs, 7b and 7c. This is mainly because the shear stresses were counteracted by more number of bars and the presence of BMF that act as dowels. The distance between cracks and their total number in BFRC slabs ranged from 40 mm to 80 mm and 30 to 40, respectively, whereas in plain concrete slabs it ranged from 60 mm to 100 mm and 23 to 27. This observation might be attributed to the bridging action of BMF across cracks which results in transferring tensile stresses from BMF to the adjacent concrete sections, leading to better stress distribution and the formulation of more cracks. Test findings also demonstrated that slabs with a higher reinforcement ratio failed in a more brittle manner than slabs with a lower reinforcement ratio due to their failure under higher stresses. The same observation was noticed for plain concrete slabs when compared to their counterpart slabs with 0.75 % BMF since the BMF allows the formulation of multiple cracks distributed along the shear span rather than localized at one location, which delays the development of major cracks that can cause brittle collapsing and leads to a less brittle shear failure.

3.2.4. The shear capacity

As illustrated in Fig. 4, the shear capacity of the tested slabs varied when different types of FRP bars were used. Slab SCG-ρ1-0 % with GFRP bars showed higher shear capacity than slabs RB-ρ1-0 % and SCB-ρ1-0 % by 8 % and 18 %, respectively. As discussed earlier, this difference could be caused by the variation in the actual bar diameters for different types of FRP bars listed in Table 2, which induced a bigger surface area of friction with the surrounding concrete that retarded the cracks widening and preserved higher shear capacity. Fig. 7a shows that the shear crack in slab SCB-ρ1-0 % exhibited an increased rate of widening at a loading level of 125 kN, whereas slabs SGB-ρ1-0 % and RB-ρ1-0 % delayed the shear crack widening up to loading levels of 165 kN and 152 kN, respectively.

In addition, Fig. 4b revealed that there is a clear trend of increasing the shear capacity as the reinforcement ratio increased from 0.792 % to 1.27 %. Slab SCB-ρ2-0 % has shown 29 % increase in the ultimate shear capacity over its counterpart slab SCB-ρ1-0 %. Similarly, slab RB-ρ2-0 % has shown 25 % increase in the ultimate shear capacity over its counterpart slab RB-ρ1-0 %. In their study, El-sayed et al. [1] related such an observation to the reduced width and penetration depth of the shear crack, which will improve the contribution of aggregate interlock and the uncracked concrete in compression. This has been proved from the shear crack widths results presented in Fig. 7b, where at a loading level of 150 kN, the shear crack width of slab RB-ρ2-0 % reached 0.38 mm before being restrained from widening until reaching a higher loading capacity, whereas the shear crack width of slab RB-ρ1-0 % at the same loading stage reached 2.3 mm. This has caused a drop in the load followed by a significant increase in the crack width until reaching 7 mm, causing the slab to fail in shear. Additionally, the increased shear capacity when using a higher area of flexural reinforcing bars could be related to the improved dowel capacity which induces less tensile
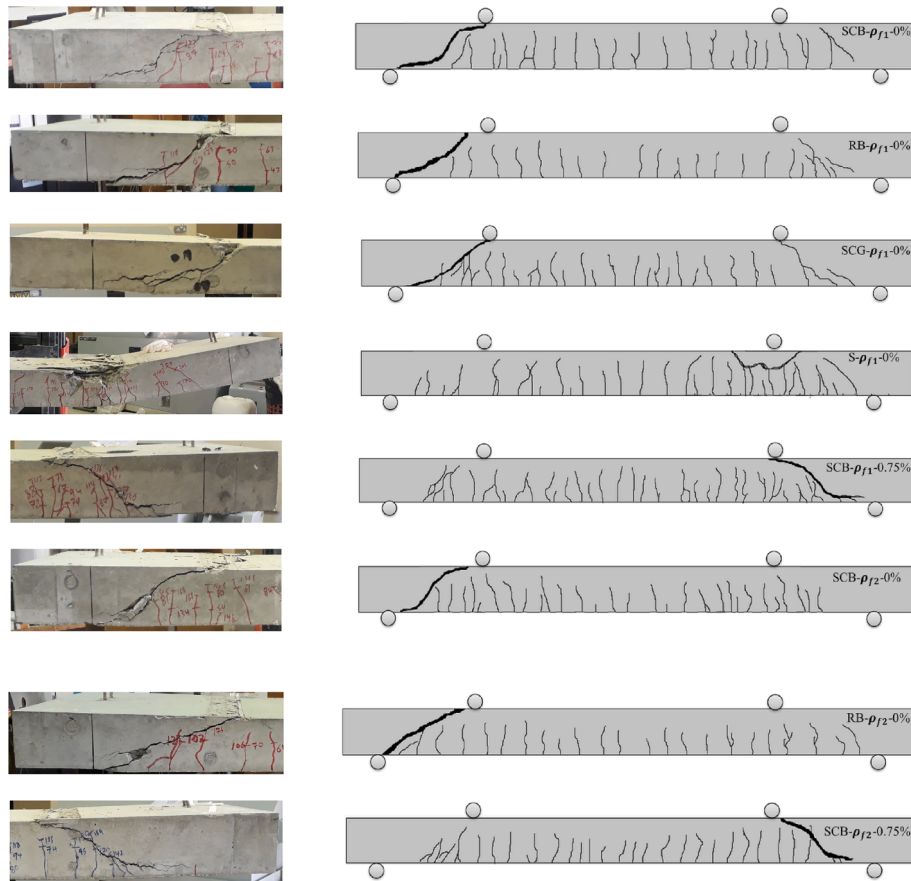
Fig. 6. Failure modes and cracks pattern.

stresses in the surrounded concrete[1]. It is worth mentioning that the effect of flexural reinforcement is not governed by the reinforcement ratio only but the axial stiffness (ρE) as well, where E is the elastic modulus of the bar. This observation can be clearly noticed in Fig. 4a and 4b, where the control slab S-ρ1-0 % reinforced with steel experienced a much higher toughness with a 32 % to 57 % higher ultimate loading capacity than its counterpart slabs SCB-ρ1-0 %, RB-ρ1-0 %, and SCG-ρ1-0 %. Furthermore, even though slabs SCB-ρ2-0 % and RB-ρ2-0 % had a 60 % higher reinforcement ratio than the control slab S-ρ1-0 %, the control slab has shown 14.6 % to 21 % higher ultimate loading capacity with higher stiffness. Similar findings were reported El-Sayed et al. [1] who reported that the axial stiffness was determined as the sole factor that governs the effect of flexural reinforcement on shear capacity.

The incorporation of 0.75 % of BMF was also effective in enhancing slabs' shear capacity. The ultimate shear capacity of slab SCB-ρ1-0.75 % was enhanced by 16.7 % when compared to the control slab SCB-ρ1-0 %. Fig. 7c demonstrated that slab SCB-ρ1-0 % encountered a shear crack width of 2 mm at a loading level of 140 kN compared to a width of 0.33 mm in slab SCB-ρ1-0.75 %. As a result, the random distribution of the BMF in the concrete mix (See Fig. 8) has resulted in an additional shear resisting component across the diagonal shear crack as shown in Fig. 9. Also, the added fibers enhance the tensile strength of concrete in the tension zone. Consequently, this requires a larger compression zone to satisfy the horizontal equilibrium in the FRP-RC cross-section. Thus, the contribution to shear resistance resulting from the uncracked concrete in the compression zone is expected to increase due to the addition of BMF. Another possible reason for the enhanced shear capacity caused by the added BMF is the improved dowel action in BFRC slabs. According to Lantsoght [42], the dowel action resistance, at maximum, depends on the tensile strength of concrete cover, which fails through splitting when

large tensile dowel forces around the reinforcing bars are generated. However, the effect of BMF was less pronounced in the slab with a higher reinforcement ratio. For instance, slab SCB-ρ2-0.75 % exhibited only a 4 % increase in the ultimate shear capacity over slab SCB-ρ2-0 %, which indicates that the shear behavior is governed by the reinforcing bars at higher reinforcement ratios.

4. Analytical investigation

Based on the available methodologies utilized in current codes and design guidelines, the shear capacity of FRC sections could be calculated using either of two approaches: (1) calculating the individual shear contribution approach from concrete and fibers; or (2) suggesting a direct modification to the concrete shear contribution due to the addition of fibers. In this section, the shear capacity of the tested slabs was predicted using both approaches.

4.1. Concrete contribution to shear resistance

In this section, 33 FRP reinforced slabs collected from previous studies [1,11,31], in addition to the slabs in the current study, were predicted using the theoretical shear models of different design codes, guidelines, and other researchers listed in Table 6. For each model, the ratio of experimental shear capacity to predicted shear capacity V_{exp}/V_{pre}, the standard deviation (SD), and the coefficient of variation (COV%) were calculated in Table 7. Moreover, the effect of f_c', a/d, and ρ on the ratio of V_{exp}/V_{pre} was investigated as indicated in Figs. 10 and 11. According to Table 7 and Fig. 10, the average values of V_{exp}/V_{pre} revealed that the design codes and guidelines have underestimated the experimental shear capacities with *ACI* 440.1R-15 [7] having the most conservative predictions among the rest of the models. Hence, for design
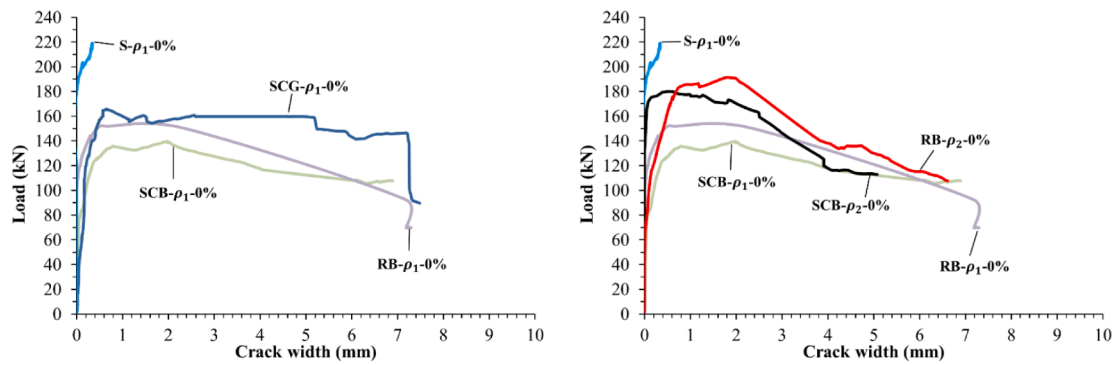
(a) Effect of reinforcement type

(b) Effect of reinforcement ratio
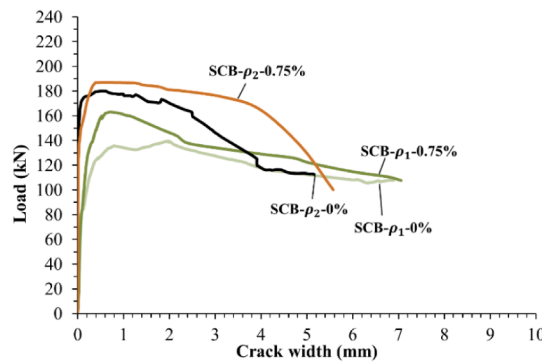
(c) Effect of V_f of BMF

Fig. 7. Load vs crack width behavior of the tested slabs.

Fig. 8. BMF distribution in the fresh concrete.

purposes, the *ACI* 440.1R-15 [7] seems to be not economic as stated by Hosseini et al. [43]. On the contrary, some of the predictions were overestimated by ISIS-2007 [10], especially at ρ levels of less than 1 % and a/d ratios greater than 5. These inaccurate predictions might be related to

the exclusion of ρ and a/d terms in Eq. (4) of the ISIS-2007 [10] code, which therefore leads to a higher scattering of data points with COV% of 29.23. Furthermore, the proposed models of Wegian and Abdalla (2005) [44] and Alam and Hussein (2013) [45] were noticed to show unsafe
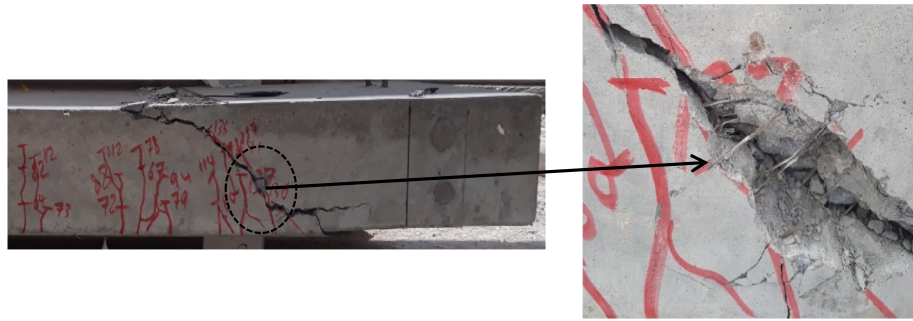
Fig. 9. BMF bridging the shear crack.

Table 6
Current models for predicting the shear strength of one-way slabs reinforced with FRP bars.

Reference	Model	Equation No.
ACI 440.1R-15 [7]	$V_c = \frac{2}{5}\sqrt{f'c}\,b_w kd$ $k = \sqrt{2\rho n + (\rho n)^2} - \rho n$ $b_w = section\ width$ $d = section\ effective\ depth$ $n = ratio\ of\ modulus\ of\ elasticity\ of\ FRP\ bars\ (E_f)\ to\ the\ modulus\ of\ elasticity\ of\ concrete\ (E_c)$	Eq (1)
CAN/CSA-S806-12[8]	$V_c = 0.05\lambda k_m k_r (f'c)^{\frac{1}{3}} b_w d_v, for\ d \leq 300mm$ $where\ 0.11\sqrt{f'c}\,b_w d_v \leq V_c \leq 0.22\sqrt{f'c}\,b_w d_v$ $d_v = 0.9 \times section\ height(h)$ $k_m = \sqrt{\frac{V_f d}{M_f}} \leq 1.0, where \left(\frac{V_f d}{M_f}\right)\ is\ equivalent\ to\ \left(\frac{d}{a}\right)$ $V_f = ultimate\ shear\ capacity$ $M_f = ultimate\ moment\ capacity$ $k_r = 1 + (E_f\rho)^{\frac{1}{3}}$	Eq (2)
JSCE-1997[9]	$V_c = \beta_d\beta_p\beta_n f_{vcd} b_w d / \gamma_b$ $\beta_d = \left(\frac{1000}{d}\right)^{\frac{1}{4}} \leq 1.5\ \beta_p = \left(\frac{1000\rho E}{E_s}\right)^{\frac{1}{4}} \leq 1.5$ $\beta_n = 1\ if\ no\ axial\ force\ applied\ f_{vcd} = 0.2\sqrt[3]{f'c}\ provided\ that\ f_{vcd} \leq 0.72\frac{N}{mm^2}$ $\gamma_b = 1$	Eq (3)
ISIS-2007 [10]	$V_c = 0.2\lambda\sqrt{f'c}\,cb_w d\sqrt{\frac{E_f}{E_s}}$ $E_s = Elastic\ modulus\ for\ steel$	Eq (4)
Wegian and Abdalla (2005)[44]	$V_c = 2\left(f'_c\frac{\rho E_f}{E_s}\frac{d}{a}\right)^{\frac{1}{3}} b_w d$	Eq (5)
Razaqpur and Isgor (2006)[46]	$V_c = 0.035 k_m k_s k_a [1 + k_r]\sqrt{f'_c}\ b_w d$ $where\ k_m = \left(\frac{V_f d}{M_f}\right)^{\frac{2}{3}},\ k_r = (\rho E_f)^{\frac{1}{3}}$ $k_s = \begin{cases} 1\ for\ d \leq 300mm \\ \frac{750}{450+d} for\ d > 300mm \end{cases}$ $k_a = \begin{cases} 1\ for\ \frac{M_f}{V_f d} \geq 2.5 \\ \frac{2.5}{\frac{M_f}{V_f d}} \leq 2.5\ for\ \frac{M_f}{V_f d} < 2.5 \end{cases}$	Eq (6)
Alam and Hussein (2013)[45]	$V_c = \frac{0.2\lambda}{\left(\frac{a}{d}\right)^{\frac{2}{3}}}\left(\frac{\rho E_f}{d}\right)^{\frac{1}{3}}\sqrt{f'_c}\ b_w d$ $Where\ \frac{0.1\lambda}{a/d}\sqrt{f'_c}\ b_w d \leq V_c \leq 0.2\lambda\sqrt{f'_c}\ b_w d$	Eq (7)
Kim and Jang (2014)[47]	$V_c = \beta_f\frac{1}{6}\sqrt{f'_c}\ b_w d$ $where:\ \frac{a}{d} \leq 2.5;\ \beta_f = 3.944 + 0.256\left(\frac{E_f}{E_s}\right) - 1.472\frac{a}{d} + 73.886\rho$ $\frac{a}{d} > 2.5;\ \beta_f = 0.716 + 0.466\left(\frac{E_f}{E_s}\right) - 0.095\frac{a}{d} + 32.101\rho$	Eq (8)

Table 7
Comparison of the experimental shear capacity of previously and currently tested slabs with the available design standards and guidelines.

Source	Bar type	ρ(%)	b_w (mm)	h (mm)	a (mm)	f'_c (MPa)	E_{frp} (GPa)	f_{fu} (MPa)	Experimental Shear, V_c (kN)	ACI-440–15 V_{exp}/V_{pre}	JSCE-1997 V_{exp}/V_{pre}	CAN/CSA-S806-12 V_{exp}/V_{pre}	ISIS-2007 V_{exp}/V_{pre}	Wegian and Abdalla (2005) V_{exp}/V_{pre}	Razaqpor and Isgor (2006) V_{exp}/V_{pre}	Alam and Hussein (2013) V_{exp}/V_{pre}	Kim and Jang (2014) V_{exp}/V_{pre}
El-sayed, El-salakawy, and Benmokrane [1]	CFRP	0.39	1000	200	1000	40	114	1536	140	2.13	1.38	1.37	0.90	0.96	1.50	0.95	1.54
		0.78	1000	200	1000	40	114	1536	167	1.86	1.30	1.55	1.07	0.91	1.45	0.90	1.49
		1.18	1000	200	1000	40	114	1536	190	1.79	1.30	1.57	1.23	0.91	1.48	0.90	1.43
	GFRP	0.86	1000	200	1000	40	40	597	113	1.96	1.23	1.12	1.24	0.85	1.33	0.85	1.33
		1.7	1000	200	1000	40	40	540	142	1.83	1.24	1.42	1.57	0.87	1.40	0.86	1.11
		1.71	1000	200	1000	40	40	597	163	2.06	1.40	1.60	1.77	0.97	1.55	0.96	1.23
		2.44	1000	200	1000	40	40	540	163	1.80	1.27	1.54	1.82	0.89	1.45	0.88	0.98
		2.63	1000	200	1000	40	40	597	168	1.80	1.28	1.55	1.87	0.89	1.46	0.89	0.95
Abdulsalam, Farghaly and Benmokrane [31]	CFRP	0.52	1000	200	850	49.7	144	1899	119	1.81	1.26	1.40	0.82	0.86	1.43	0.81	1.50
		0.62	1000	200	850	49.6	144	1899	141	1.97	1.39	1.65	0.96	0.95	1.60	0.90	1.66
		0.72	1000	200	850	52	144	1899	159	2.05	1.49	1.81	1.05	1.00	1.67	0.93	1.71
		0.83	1000	200	850	44.8	144	1899	157	2.00	1.43	1.83	1.13	1.00	1.72	0.96	1.76
		0.94	1000	200	850	45.6	140	1648	173	2.03	1.46	1.84	1.21	1.02	1.72	1.01	1.72
		1.10	1000	200	850	48.6	140	1648	186	2.01	1.49	1.85	1.26	1.02	1.71	1.06	1.68
		1.25	1000	200	850	41.3	140	1648	192	2.04	1.52	1.92	1.40	1.06	1.83	1.18	1.75
		0.72	1000	200	850	76	144	1899	168	1.95	1.57	1.58	0.92	0.93	1.46	0.82	1.50
		0.72	1000	200	850	86.2	144	1899	137	1.53	1.28	1.21	0.71	0.73	1.12	0.62	1.15
Abdul-salam, Sabry and Benmokrane [11]	GFRP	1.00	1000	200	850	47.9	40.8	724	94	1.63	1.04	0.97	1.06	0.72	1.06	0.65	1.01
		0.80	1000	200	850	48.4	49.8	666	106	1.85	1.18	1.08	1.07	0.81	1.20	0.73	1.23
		1.10	1000	200	850	42.9	67.8	1197	155	2.13	1.46	1.70	1.44	1.01	1.58	0.93	1.54
		1.10	1000	200	850	77.4	67.8	1197	163	1.90	1.49	1.33	1.13	0.88	1.24	0.73	1.21
		1.10	1000	200	850	82.6	67.8	1197	145	1.66	1.32	1.14	0.97	0.76	1.07	0.63	1.04
	CFRP	0.51	1000	200	850	49.7	139.2	1906	119	1.56	1.07	1.18	0.70	0.73	1.09	0.65	1.08
	GFRP	1.85	1000	200	850	47.9	43.9	588	121	1.60	1.10	1.29	1.36	0.76	1.19	0.70	0.93
		1.10	1000	200	850	42.9	67.8	1197	155	2.13	1.46	1.70	1.44	1.01	1.58	0.93	1.54
		1.30	1000	200	850	49.4	67.8	1197	167	2.02	1.42	1.63	1.43	0.97	1.47	0.87	1.37
	CFRP	0.62	1000	200	850	49.4	147.8	1906	141	1.67	1.18	1.36	0.82	0.81	1.23	0.72	1.21
		0.72	1000	200	850	52.0	144.0	1906	159	1.75	1.28	1.44	0.90	0.86	1.29	0.76	1.28
		0.72	1000	200	850	76.0	144.0	1906	168	1.67	1.35	1.34	0.79	0.80	1.13	0.66	1.12
		0.72	1000	200	850	86.2	144.0	1906	137	1.31	1.10	1.04	0.60	0.62	0.86	0.51	0.85
		1.25	1000	200	850	41.3	141.0	1680	192	1.82	1.36	1.62	1.25	0.95	1.51	0.87	1.43
	GFRP	2.62	1000	200	850	48.6	67.8	1197	170	1.54	1.15	1.36	1.48	0.79	1.24	0.71	0.90
		3.78	1000	200	850	50.3	65.4	1078	213	1.75	1.36	1.64	1.95	0.93	1.49	0.84	0.90
Current study	BFRP	0.76	600	150	400	55.12	49.48	1177	69.82	2.45	1.58	1.30	1.36	1.06	1.00	0.61	1.08
		0.76	600	150	400	55.12	50	1100	76.18	2.66	1.72	1.41	1.48	1.15	1.09	0.66	1.17
	GFRP	0.76	600	150	400	55.12	43.65	1030	82.96	3.09	1.96	1.60	1.72	1.31	1.23	0.75	1.30
	BFRP	0.76	600	150	400	55.33	49.48	1177	81.48	2.86	1.84	1.52	1.59	1.24	1.23	0.71	1.26
		1.2	600	150	400	55.12	49.48	1177	90.08	2.57	1.75	1.46	1.76	1.18	1.13	0.67	1.17
		1.2	600	150	400	55.12	50	1100	95.65	2.71	1.85	1.55	1.86	1.24	1.20	0.71	1.24
		1.2	600	150	400	55.33	49.48	1177	93.55	2.66	1.82	1.52	1.83	1.22	1.24	0.70	1.22
Mean										1.99	1.40	1.47	1.27	0.94	1.36	0.80	1.29
SD										0.39	0.22	0.23	0.37	0.16	0.22	0.14	0.26
COV%										19.74	15.99	15.93	29.23	16.87	16.35	17.67	20.16

E_{frp}: Modulus of elasticity of FRP bar; f_{fu}: Ultimate tensile strength of FRP bar.
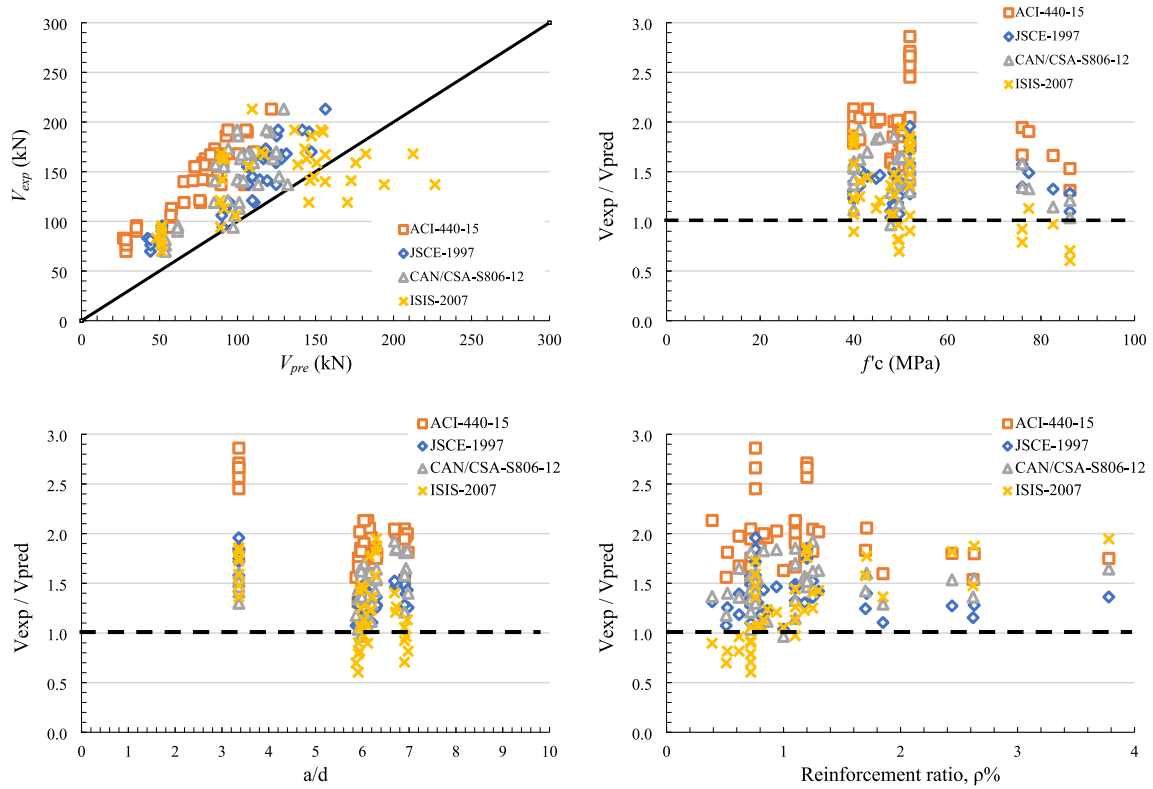
Fig. 10. Experimental vs predicted shear capacities using design codes and guidelines.
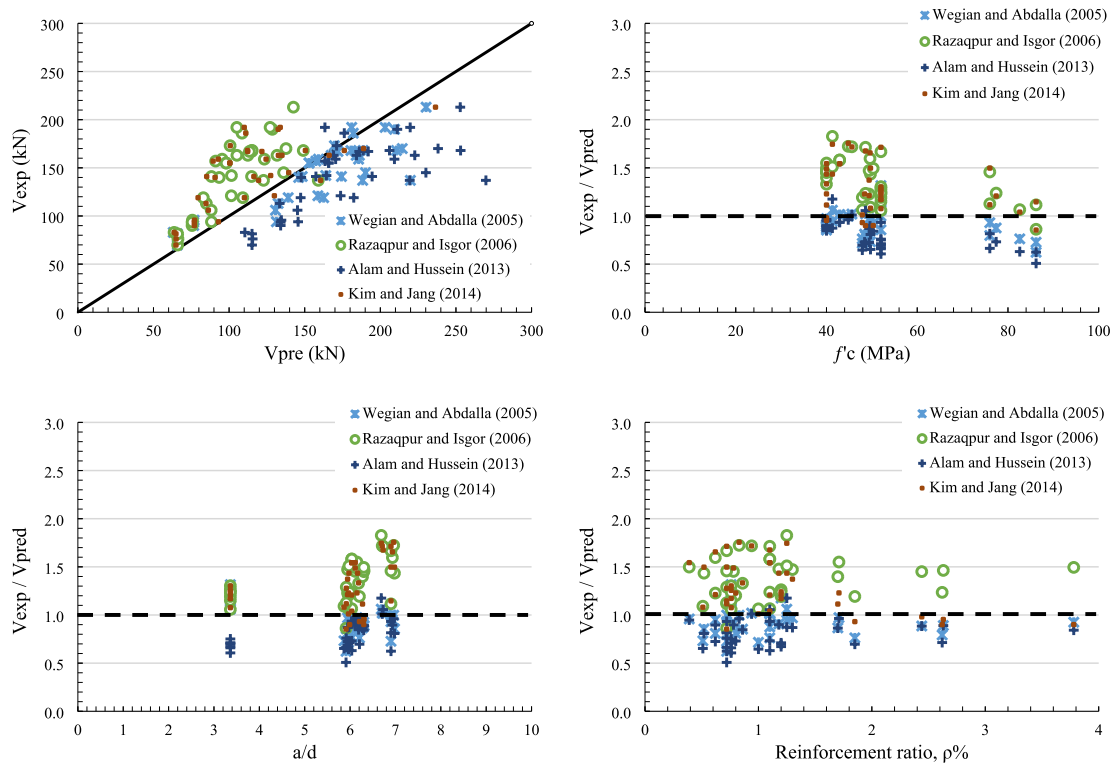

Fig. 11. Experimental vs predicted shear capacities using existing models in the literature.
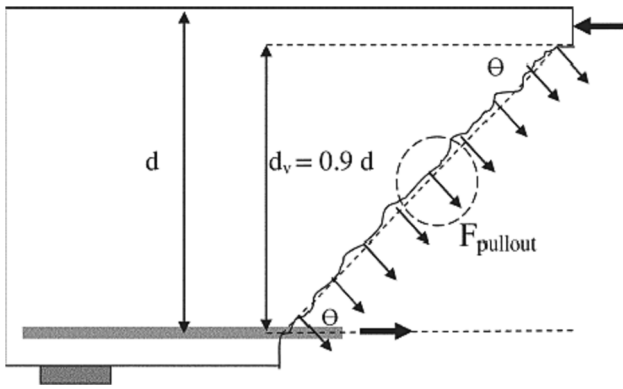
Fig. 12. Macro fibers contribution to shear resistance according to Aoude et al[48].

predictions for most of the slabs presented in Table 7, while the models of Razaqpur and Isgor (2006) [46] and Kim and Jang (2014) [47] showed safe predictions with acceptable precision of the tested slabs. However, as can be seen in Table 7 and Fig. 11, the model of Kim and Jang (2014) [47] was found to over-estimate the shear capacity for slabs with a reinforcement ratio equal to or above 1.85 %, therefore, the model of Razaqpur and Isgor (2006) [46] will be nominated to predict the plain concrete contribution to shear strength of FRP reinforced slabs.

4.2. BMF contribution to shear resistance

As shown in Fig. 12, the increase in shear resistance of concrete slabs due to the addition of BMF is mainly related to fibers crossing the inclined crack of angle θ and keeps carrying tensile stresses until fibers ruptured or pulled out. The BMF contribution to shear strength (V_{fib}), as suggested by Aoude et al. [48] for steel fibers, can be calculated according to Eq. (9), but in this study the term $\sqrt{\frac{E_{fiber}}{E_s}}$ is added to take into account the reduction due to the use of BMF instead of steel fibers:

$$V_{fib} = \left(N_{fib} \times 0.83 F_p \sqrt{\frac{E_{fiber}}{E_s}} \right) \times b_w d_v \times cot\theta \qquad (9)$$

where E_{fiber} is the modulus of elasticity for the used fibers, E_s is the modulus of elasticity for steel fibers, and N_{fib} is the effective number of fibers crossing a unit area of the cracked plane and it is calculated as in Eq. (10):

$$N_{fib} = \frac{V_f}{\frac{\pi}{4} \times d_f^2} \times \alpha \times \eta_l \qquad (10)$$

where α and η_l were taken as 3/8 [49] and 0.5 [50], respectively, to account for the random orientation of fibers and the variability of the embedment length crossing any cracked surface of the concrete matrix.

The term F_p represents the BMF pull-out strength and can be found as in Eq. (11):

$$F_p = \tau \times \pi \times d_f \times \frac{l_f}{4} \qquad (11)$$

where $\frac{l_f}{4}$ is the mean pull-out length [51], and τ is the shear-bond strength which in the case of BMF, Adhikari [51] suggested Eq. (12) to calculate it as follow:

$$\tau = \frac{\sigma_f \times d_f}{4 \times l_f} \qquad (12)$$

The angle θ can be determined experimentally and if not, Eq. (13) can be used as follow:

$$\theta = (\varepsilon_x \times 7000) + 29° \qquad (13)$$

Where $30 \leq \theta \leq 60$, and ε_x is referred to the longitudinal strain at the mid-depth of the member's cross-section and it is determined as in Eq. (14):

$$\varepsilon_x = \frac{\left(\frac{M}{d_v}\right) + V}{2 \times E_{frp} \times A_{frp}} \qquad (14)$$

The terms M and V are the moment at a section $d_v = 0.9d$ from the point load and the maximum shear value, respectively, and A_{frp} is the cross-sectional area of longitudinal reinforcement.

As stated previously, some shear models suggest that the concrete contribution to shear strength should directly be modified when it comes to evaluating the shear capacity of FRC sections. For example, the International Federation for Structural Concrete *fib* Model Code 2010 [52] is implementing Eq. (15) to calculate the shear resistance in steel FRC members as follows:

$$V_{FRC} = \left\{ \frac{0.18}{\gamma_c} k_s \left[\left(1 + 7.5 \left(\frac{f_{ut-FRC}}{f_t} \right) \right) f_c' \right]^{\frac{1}{3}} + 0.15\sigma_{cp} \right\} b_w \bullet d \qquad (15)$$

where γ_c is a partial safety factor for concrete and was assumed as 1 in this study, $k_s = 1 + \sqrt{\frac{200}{d}} \leq 2$, f_{ut-FRC} is the residual strength value which corresponds to $0.37f_{150}^D$, f_t is the tensile strength of plain concrete which was calculated as $0.33\sqrt{f'c}$ [53], and σ_{cp} is the average normal stress acting on the concrete section.

Table 8
Comparison of experimental vs predicted shear capacities of the proposed model and the Model Code 2010.

Source	Bar type	ρ(%)	b_w (mm)	h (mm)	a/d	f'c (MPa)	E_{frp}(GPa)	f_{fu}(MPa)	V_f% of BMF	Experimental Shear,V_c(kN)	Proposed model (Eq. (6) + Eq.(9)) V_{exp}/V_{pre}	*fib* Model Code 2010[52] V_{exp}/V_{pre}
Current study	BFRP	0.76	600	150	3.36	55.12	49.48	1177	0	69.82	1.00	0.77
		0.76	600	150	3.36	55.12	50	1100	0	76.18	1.09	0.84
	GFRP	0.76	600	150	3.36	55.12	43.65	1030	0	82.96	1.23	0.91
	BFRP	0.76	600	150	3.36	55.33	49.48	1177	0.75	81.48	1.07	0.80
		1.2	600	150	3.36	55.12	49.48	1177	0	90.08	1.13	0.85
		1.2	600	150	3.36	55.12	50	1100	0	95.65	1.20	0.90
		1.2	600	150	3.36	55.33	49.48	1177	0.75	93.55	1.07	0.79
Mohaghegh et al [19]	BFRP	1.38	100	200	2	81.6	58.1	1095	0.5	45.72	0.91	1.11
		1.38	100	200	2	78.6	58.1	1095	1	43.88	1.09	1.00
		1.38	100	200	2	79.8	58.1	1095	1.33	44.77	1.14	1.01
		1.38	100	200	2	78.6	58.1	1095	1.67	44.46	1.16	0.94
		1.38	100	200	2	77	58.1	1095	2	44.50	1.16	0.98
Mean											1.10	0.91
SD											0.09	0.10
COV%											7.95	11.52

4.3. Validation of the proposed model

At this stage, the first approach, where the combination of the individual contribution of Eq. (6) and Eq. (9) is proposed, is compared to the second approach model of the *fib* Model Code 2010 [52] in Eq. (15) to predict the experimental results of the current study. For further validation of the proposed model, the results of Mohaghegh et al. [19] who tested BFRP-BFRC beams will also be evaluated. Table 8 presents the comparison between the experimental and the predicted shear capacities of the two models. The results showed that the proposed model has accurately and conservatively predicted the experimental data with a mean V_{exp}/V_{pre} of 1.10 and a low COV% of 7.95. On the other hand, the *fib* Model Code 2010[52] noticed to show unsafe predictions with a mean V_{exp}/V_{pre} of 0.91, especially for members with $a/d \geq 2.5$, whereas it was observed to provide better accuracy predictions for members with $a/d \leq 2.5$.

5. Conclusions

According to the above discussion and analysis, the main findings of this study can be summarized as follow:

1- The addition of 0.75 % of BMF had no apparent effect on the compressive strength of concrete. On the other hand, it had increased the maximum flexural tensile capacity of concrete by 17 % and resulted in a progressive declination in the bending load at the post-cracking stage. This indicates the better energy absorption capacity and the higher capability of BFRC prisms than that of plain concrete prisms to withstand the crack opening.

2- The addition of BMF resulted in a 16.7 % gain in the shear capacity of the tested slabs with a reinforcement ratio level of 0.792 %, whereas their effect was reduced to 4 % for at a higher reinforcement ratio level of 1.27 %. This indicates that the shear behavior is governed by the longitudinal reinforcing bars at higher reinforcement ratios.

3- The added BMF has restricted flexural cracks propagation and widening and leads to reduced midspan deflection and strain values for both the longitudinal BFRP bars and concrete. In addition, the BMF bridging across the shear crack surfaces has shown the tendency to reduce crack widths, thus improving the aggregate interlock contribution and delaying its failure.

4- All of the over-reinforced BFRP-RC slabs have encountered shear failure, whereas the under-reinforced steel-RC slab failed by steel yielding followed by concrete crushing. Despite the fact that BFRP-RC slabs failed under shear, the BMF addition allowed for improved stress distribution in the BFRP-BFRC slabs, resulting in the formulation of multiple cracks distributed along the shear span rather than localized at one location. This has delayed the development of major shear cracks that can cause brittle collapsing and lead to a less brittle shear failure.

5- When the reinforcement ratio was increased from 0.792 % to 1.27 %, slabs reinforced with sand-coated BFRP bars had a 29 % higher shear capacity, while the shear capacity was enhanced by 25 % for those reinforced with ribbed BFRP bars.

6- The experimental shear capacities of FRP reinforced slabs were under-estimated by the available codes and design guidelines, especially by the *ACI*-440–15, which showed the most conservative predictions. However, the ISIS-2007 [10] code was observed to over-estimate the prediction at a lower reinforcement ratio than 1 %, and at a/d ratios greater than 5. On the other hand, the proposed models of Wegian and Abdalla (2005) [44] and Alam and Hussein (2013) [45] showed unconservative predictions for most of the collected slabs, while the models of Razaqpur and Isgor (2006) [46] and Kim and Jang (2014) [47] showed conservative predictions with acceptable accuracy.

7- The proposed model in this study, which accounts for the individual contribution of concrete and the BMF, demonstrated conservative and accurate predictions for the shear capacities of the tested slabs and the tests carried out by Mohaghegh et al. [19], with a mean V_{exp}/V_{pre} of 1.10, whereas the *fib* Model Code 2010 [52] has under-estimated the shear capacity with a mean V_{exp}/V_{pre} of 0.91, especially at a/d ratio ≥ 2.5.

Declaration of Competing Interest

The authors declare that they have no known competing financial interests or personal relationships that could have appeared to influence the work reported in this paper.

Data availability

The raw/processed data required to reproduce these findings cannot be shared at this time as the data also forms part of an ongoing study.

References

[1] El-sayed A, El-salakawy E, Benmokrane B. Shear Strength of One-Way Concrete Slabs Reinforced with Fiber-Reinforced Polymer Composite Bars. J Compos Constr 2005;9:147–57. https://doi.org/10.1061/(ASCE)1090-0268(2005)9.

[2] El-Sayed AK, El-Salakawy EF, Benmokrane B. Shear capacity of high-strength concrete beams reinforced with FRP bars. ACI Struct J 2006;103:383–9. https://doi.org/10.14359/15316.

[3] El-Sayed AK, El-Salakawy EF, Benmokrane B. Shear Strength of FRP-Reinforced Concrete Beams without Transverse Reinforcement. ACI Struct J 2006;103:235–43. https://doi.org/10.14359/15181.

[4] Razaqpur AG, Isgor BO, Greenaway S, Selley A. Concrete Contribution to the Shear Resistance of Fiber Reinforced Polymer Reinforced Concrete Members. J Compos Constr 2004;8:452–60. https://doi.org/10.1061/(ASCE)1090-0268(2004)8:5 (452).

[5] Attia K, El Refai A, Alnahhal W. Flexural Behavior of Basalt Fiber-Reinforced Concrete Slab Strips with BFRP Bars: Experimental Testing and Numerical Simulation. J Compos Constr 2020;24:04020007. https://doi.org/10.1061/(ASCE) CC.1943-5614.0001002.

[6] Abushanab A, Alnahhal W, Farraj M. Structural performance and moment redistribution of basalt FRC continuous beams reinforced with basalt FRP bars. Eng Struct 2021;240:112390. https://doi.org/10.1016/j.engstruct.2021.112390.

[7] American Concrete Institute (ACI) Committee 440. Guide for the Design and Construction of Structural Concrete Reinforced with Fibre-Reinforced Polymer (FRP) Bars (ACI 440.1R-15). 2015. doi:10.1061/40753(171)158.

[8] CSA (Canadian Standards Association). Design and construction of building components with fiber reinforced polymers. (CSA-S806-12) 2012.

[9] JSCE(Japan Society of Civil Engineers). Recommendation for design and construction of concrete structures using continuous fiber reinforcing materials. 1997:1–58.

[10] Isis. Intelligent Sensing for Innovative Structures. Reinforcing Concrete Structures with Fibre Reinforced Polymers 2007.

[11] Abdul-Salam B, Farghaly AS, Benmokrane B. Mechanisms of shear resistance of one-way concrete slabs reinforced with FRP bars. Constr Build Mater 2016;127: 959–70. https://doi.org/10.1016/j.conbuildmat.2016.10.015.

[12] Momani Y, Tarawneh A, Alawadi R, Momani Z. Shear strength prediction of steel fiber-reinforced concrete beams without stirrups. Innov Infrastruct Solut 2022;7. doi:10.1007/s41062-021-00703-w.

[13] Dinh HH, Parra-montesinos GJ, Wight JK. Shear Strength Model for Steel Fiber Reinforced Concrete Beams without Stirrup Reinforcement. J Struct Eng 2011;137: 1039–51. https://doi.org/10.1061/(ASCE)ST.1943-541X.0000362.

[14] Sahoo DR, Sharma A. Effect of Steel Fiber Content on Behavior of Concrete Beams with and without Stirrups. ACI Struct J 2014;111:1157–66. https://doi.org/10.14359/51686821.

[15] Sahoo DR, Maran K, Kumar A. Effect of steel and synthetic fibers on shear strength of RC beams without shear stirrups. Constr Build Mater 2015;83:150–8. https://doi.org/10.1016/j.conbuildmat.2015.03.010.

[16] El-dieb AS, El-maaddawy TA, Al-rawashdah O. Shear behavior of ultra - high - strength steel fiber - reinforced self - compacting concrete beams. Constr Mater Struct 2014:972–9. https://doi.org/10.3233/978-1-61499-466-4-972.

[17] Ding Y, You Z, Jalali S. The composite effect of steel fibres and stirrups on the shear behaviour of beams using self-consolidating concrete. Eng Struct 2011;33:107–17. https://doi.org/10.1016/j.engstruct.2010.09.023.

[18] Amin A, Foster SJ. Shear strength of steel fibre reinforced concrete beams with stirrups. Eng Struct 2016;111:323–32. https://doi.org/10.1016/j.engstruct.2015.12.026.

[19] Mohammadi Mohaghegh A, Silfwerbrand J, Årskog V. Shear behavior of high-performance basalt fiber concrete—Part I: Laboratory shear tests on beams with macro fibers and bars. Struct Concr 2018;19:246–54. https://doi.org/10.1002/suco.201700208.

[20] Al-Hamrani A, Alnahhal W. Shear behavior of basalt FRC beams reinforced with basalt FRP bars and glass FRP stirrups: Experimental and analytical investigations. Eng Struct 2021;242:112612. https://doi.org/10.1016/j.engstruct.2021.112612.

[21] El Refai A, Alnahhal W, Al-Hamrani A, Hamed S. Shear performance of basalt fiber-reinforced concrete beams reinforced with BFRP bars. Compos Struct 2022;288: 115443. https://doi.org/10.1016/j.compstruct.2022.115443.

[22] Alnahhal W, Taha R, Alnuaimi N, Al-Hamrani A. Properties of fibre-reinforced concrete made with discarded materials. Mag Concr Res 2019;71(3):152–62. https://doi.org/10.1680/jmacr.17.00293.

[23] Bajaj S. Effect of Corrossion on Physical and Mechanical Properties of Reinforced Concrete. University of Akron; 2012. Master thesis.

[24] High C, Seliem HM, El-Safty A, Rizkalla SH. Use of basalt fibers for concrete structures. Constr Build Mater 2015;96:37–46. https://doi.org/10.1016/j.conbuildmat.2015.07.138.

[25] Michaluk CR, Rizkalla SH, Tadros G, Benmokrane B. Flexural behavior of one-way concrete slabs reinforced by fiber reinforced plastic reinforcements. ACI Struct J 1998;95:353–65. https://doi.org/10.14359/552.

[26] Chang K, Seo D. Behavior of one-way concrete slabs reinforced with GFRP bars. J Asian Archit Build Eng 2012;11:351–8. https://doi.org/10.3130/jaabe.11.351.

[27] Benmokrane B, El-salakawy E, Cherrak Z, Wiseman A. Fibre reinforced polymer composite bars for the structural concrete slabs of a Public Works and Government Services Canada parking garage 2005;748:732–48. https://doi.org/10.1139/L04-049.

[28] Dhipanaravind, S Sivagamasundari R. Flexural Behaviour of Concrete Oneway Slabs Reinforced with Hybrid FRP Bars. Int J Appl Eng Res 2018;13:4807–15.

[29] Attia K, Alnahhal W, Elrefai A, Rihan Y. Flexural behavior of basalt fiber-reinforced concrete slab strips reinforced with BFRP and GFRP bars. Compos Struct 2019;211: 1–12. https://doi.org/10.1016/j.compstruct.2018.12.016.

[30] Zheng Y, Zhou L, Taylor SE, Ma H. Serviceability of one-way high-volume fly ash-self-compacting concrete slabs reinforced with basalt FRP bars. Constr Build Mater 2019;217:108–27. https://doi.org/10.1016/j.conbuildmat.2019.05.044.

[31] Abdulsalam B, Farghaly A, Benmokrane B. Evaluation of Shear Behavior for One-Way Concrete Slabs Reinforced with Carbon-FRP Bars. CSCE 2013 Gen. Conf. - Congrès général 2013 la SCGC, Montréal, Québec: 2013. doi:10.13140/RG.2.1.3831.7609.

[32] MST-BAR 2017.

[33] ASTM D7205/D7205M − 21. Standard Test Method for Tensile Properties of Fiber Reinforced Polymer Matrix Composite Bars. 2010. doi:10.1520/D7205.

[34] ASTM C39/C39M − 21. Standard Test Method for Compressive Strength of Cylindrical Concrete Specimens. 2001. doi:10.1520/C0039.

[35] ASTM C1609/C1609M − 19a. Standard Test Method for Flexural Performance of Fiber-Reinforced Concrete (Using Beam With Third-Point Loading). 2005. doi:10.1520/C1609.

[36] Boulekbache B, Hamrat M, Chemrouk M, Amziane S. Influence of yield stress and compressive strength on direct shear behaviour of steel fibre-reinforced concrete. Constr Build Mater 2012;27:6–14. https://doi.org/10.1016/j.conbuildmat.2011.07.015.

[37] Tahenni T, Chemrouk M, Lecompte T. Effect of steel fibers on the shear behavior of high strength concrete beams. Constr Build Mater 2016;105:14–28. https://doi.org/10.1016/j.conbuildmat.2015.12.010.

[38] F. M. Fahmy M, Shehab SE, Wu Z. Bar surface treatment effect on the bond-slip behavior and mechanism of basalt FRP bars embedded in concrete. Constr Build Mater 2021;289. doi:10.1016/j.conbuildmat.2021.122844.

[39] Faisal W. Shear Behavior of Reinforced Idgh-Strength Concrete Beams Without Shear Reinforcement. Eng J Qatar Univ 1994;7:91–113. doi:http://hdl.handle.net/10576/7808.

[40] Nilson AH. Design implications of current research on high-strength concrete. Am Concr Institute, ACI Spec Publ 1985;SP-087:85–118..

[41] Huber T, Huber P, Kollegger J. Influence of aggregate interlock on the shear resistance of reinforced concrete beams without stirrups. Eng Struct 2019;186: 26–42. https://doi.org/10.1016/j.engstruct.2019.01.074.

[42] Lantsoght EOL. How do steel fibers improve the shear capacity of reinforced concrete beams without stirrups? Compos Part B Eng 2019;175. doi:10.1016/j.compositesb.2019.107079.

[43] Hosseini SA, Nematzadeh M, Chastre C. Prediction of shear behavior of steel fiber-reinforced rubberized concrete beams reinforced with glass fiber-reinforced polymer (GFRP) bars. Compos Struct 2021;256. doi:10.1016/j.compstruct.2020.113010.

[44] Wegian FM, Abdalla HA. Shear capacity of concrete beams reinforced with fiber reinforced polymers. Compos Struct 2005;71:130–8. https://doi.org/10.1016/j.compstruct.2004.10.001.

[45] Alam MS, Hussein A. Unified Shear Design Equation for Concrete Members Reinforced with Fiber-Reinforced Polymer without Stirrups. J Compos Constr 2013;17:575–83. https://doi.org/10.1061/(asce)cc.1943-5614.0000342.

[46] Razaqpur AG, Isgor OB. Proposed shear design method for FRP-reinforced concrete members without stirrups. ACI Struct J 2006;103:908.

[47] Kim CH, Jang HS. Concrete Shear Strength of Normal and Lightweight Concrete Beams Reinforced with FRP Bars. J Compos Constr 2014;18:04013038. https://doi.org/10.1061/(ASCE)CC.1943-5614.0000440.

[48] Aoude H, Belghiti M, Cook WD, Mitchell D. Response of steel fiber-reinforced concrete beams with and without stirrups. ACI Struct J 2012;109:359–67. https://doi.org/10.14359/51683749.

[49] Foster SJ. On behavior of high-strength concrete columns: Cover spalling, steel fibers, and ductility. ACI Struct J 2001;98:583–9. https://doi.org/10.14359/10301.

[50] Aoude H. Structural Behaviour of Steel Fibre. Department of Civil Engineering and Applied Mechanics. Montreal, QC, Canada: McGill University; 2007.

[51] Adhikari S. Mechanical and structural characterization of mini-bar reinforced concrete beams 2013.

[52] International Federation for Structural Concrete (fib). Model Code 2010, Final draft, Volume 2, fib Bulletin, Vol. 66. Lausanne, Switzerland: 2012.

[53] Genikomsou AS, Polak MA. Finite element analysis of punching shear of concrete slabs using damaged plasticity model in ABAQUS. Eng Struct 2015;98:38–48. https://doi.org/10.1016/j.engstruct.2015.04.016.